Disorder Suppresses Chaos in Viscoelastic Flows

Derek M. Walkama,[1,2] Nicolas Waisbord,[1] and Jeffrey S. Guasto[1,*]
[1]Department of Mechanical Engineering, Tufts University, 200 College Avenue, Medford, Massachusetts 02155, USA
[2]Department of Physics and Astronomy, Tufts University, 574 Boston Avenue, Medford, Massachusetts 02155, USA

(Received 11 July 2019; revised manuscript received 24 December 2019; accepted 23 March 2020; published 20 April 2020)

Viscoelastic flows through microstructured geometries transition from steady to time dependent and chaotic dynamics under critical flow conditions. However, the implications of geometric disorder for flow stability are unknown. We measure the onset of spatiotemporal velocity fluctuations for a viscoelastic flow through microfluidic pillar arrays, having controlled variations of geometric disorder. Introducing a small perturbation into the pillar array (∼10% of the lattice constant) delays the onset of the instability to higher flow speed, and yet larger disorders (≥ 25%) suppress the transition to chaos. We show that disorder introduces preferential flow paths that promote shear over extensional deformation and enhance flow stability by locally reducing polymer stretching.

DOI: 10.1103/PhysRevLett.124.164501

Viscoelastic fluids encompass a wide range of complex materials having a mechanical response to strain that lies between elastic solids and viscous fluids [1]. Even in the absence of inertia, viscoelastic flows can spontaneously exhibit time dependency when elastic stresses overcome viscous stresses. This condition is often characterized by a Weissenberg number, $\mathrm{Wi} = \tau\dot{\gamma} > \mathrm{Wi}_{\mathrm{cr}} \sim 1$, where $\dot{\gamma}$ is the typical shear rate and τ is the fluid relaxation time [2]. These viscoelastic instabilities impact a wide range of natural and industrial applications, including secondary flows in DNA and blood suspensions [3,4], increased hydrodynamic resistance [5] along with power consumption and cost in polymer processing, and enhanced mixing and dispersion in microfluidic and porous media flows [6–8].

Parallel viscoelastic flows are nonlinearly unstable [9,10] and upstream flow perturbations are required to trigger a subcritical transition [11,12], where the resulting velocity fluctuations are commonly termed "elastic turbulence" [13]. Conversely, in flows with strong base curvature, a linear instability—initiated through polymer stretching along curved streamlines [14]—results in a supercritical transition [15,16]. Focusing on the latter case for flows through geometrically complex microstructure (e.g., porous media and pillar arrays) [17], time dependent, curvature-induced flow instabilities at the pore scale [18,19] communicate with adjacent pores in highly connected networks to exacerbate fluctuations. Experimental [15,20–23] and numerical [24–26] efforts have characterized elastic instabilities in a wide range of geometries, but how geometrical disorder affects the onset of elastic instability remains an open question.

Geometrical disorder is a fundamental determinant of transport properties for diverse physical systems, ranging from Anderson localization [27] to colloidal glasses [28] to network dynamics [29]. Similar to viscoelastic flows, coupled dynamical systems are known to display chaotic dynamics under sufficient driving force [30]. However, simulations suggest that disorder can promote synchronization among arrays of forced, coupled pendula [30,31] and cause a transition from a self-organized-critical (SOC) distribution of avalanches to systemwide, periodic events in earthquakes and neural networks [32,33], phenomena which have been realized in relatively few experimental systems [31,34]. In this Letter, we use microfluidic experiments to demonstrate how flow channelization, conferred by geometric disorder, suppresses the supercritical transition and chaotic dynamics of viscoelastic flow (Fig. 1). The underlying mechanism of enhanced flow stability is the promotion of shear over extensional deformation, which reduces polymer stretching. The sensitivity of this transition to small geometrical perturbations shows that the onset of linear viscoelastic instabilities in hydraulic networks is not predicted by traditional metrics [14] such as the Weissenberg number. Rather, viscoelastic stability depends strongly upon the Lagrangian deformation experienced by fluid particles, mediated by disorder. This newfound insight into viscoelastic flow stability in complex geometries has direct implications for remediation, extraction, and filtration processes, including enhanced oil recovery where chaotic viscoelastic flow promotes mixing and oil displacement [7,8].

Microfluidic channels (25 mm long, 4 mm wide, 50 μm high) containing arrays of cylindrical pillars (diameter, $d = 50$ μm) were fabricated using soft lithography. Five individual microchannels were fabricated with disorders, $\beta = [0, 0.125, 0.25, 0.5, 1.0]$, where pillar locations were randomly displaced from an ordered hexagonal lattice (lattice constant, $a = 120$ μm) within a hexagon of circumradius, βa (see Supplemental Material [35]). The viscoelastic

 © 2020 American Physical Society

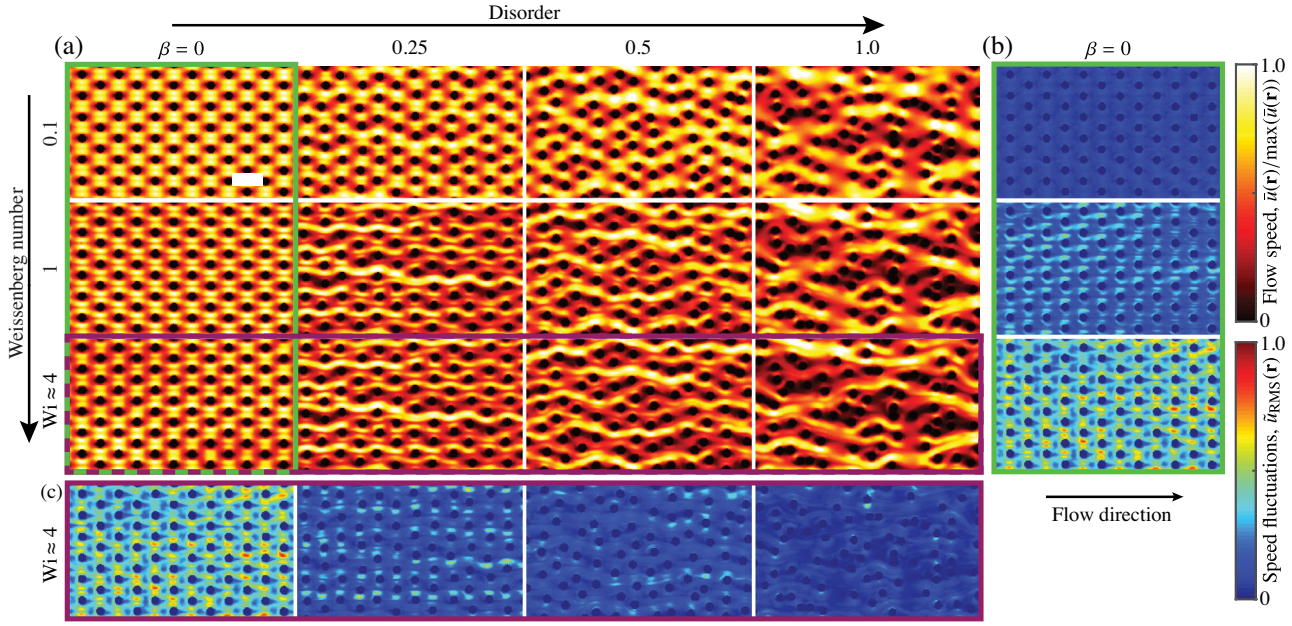

FIG. 1. Disorder reduces chaotic fluctuations in viscoelastic flows. (a) Normalized, time-averaged speed field, $\bar{u}(\mathbf{r})/\max[\bar{u}(\mathbf{r})]$, in a microfluidic pillar array for a range of Weissenberg numbers, Wi, and geometric disorders, β (40% of full field of view shown; see also Supplemental Movies 1–5 [35]). Scale bar, 150 μm. (b) Local, normalized speed field fluctuations, $\tilde{u}_{\mathrm{rms}}(\mathbf{r})$, as a function of increasing Wi, corresponding to speed fields for $\beta = 0$ [green box in (a)]. (c) Local, normalized speed fluctuations as a function of increasing disorder, corresponding to speed fields for $\mathrm{Wi} \approx 4$ [magenta box in (a)].

fluid is a dilute solution ($c/c^* = 0.43$) of high molecular weight polyacrylamide (PAA; 18×10^6 g/mol; $c =$ 150 ppm) in a viscous solvent (97% aqueous glycerol) [15]. The polymer solution is slightly shear thinning (viscosity, η) and has a relaxation time, $\tau = 1.14\,\mathrm{s} \pm 0.1\,\mathrm{s}$, where the latter was measured using a capillary breakup extensional rheometer (CaBER; see Figs. S3 and S4 [35]). The viscoelastic fluid is pressure driven through the pillar arrays (Elveflow OB1), and video microscopy (Nikon Ti-e; 10×, 0.3 NA objective) captures the motion (100 fps; Andor Zyla) of fluorescent tracer particles (diameter, 0.5 μm). Time-resolved velocity fields $\mathbf{u}(\mathbf{r}, t)$ are measured using particle image velocimetry [54], and Lagrangian statistics are obtained by simultaneous particle tracking. A maximum Reynolds number of $\mathrm{Re} = \rho U d/\eta \lesssim 10^{-4}$ (density ρ; mean flow speed U) ensures that inertial effects are negligible.

The introduction of geometric disorder into the pillar arrays shifts the flow topology from highly periodic to heterogeneous and decreases the temporal fluctuations of the velocity field. Flow speed fields, $u(\mathbf{r}, t) = |\mathbf{u}(\mathbf{r}, t)|$, are time averaged, $\bar{u}(\mathbf{r}) = \langle u(\mathbf{r}, t)\rangle_t$, to quantify flow topology [Fig. 1(a)] as a function of both disorder β and flow strength, where the latter is characterized by the Weissenberg number, $\mathrm{Wi} = \tau U/d$. At low Wi, disorder induces heterogeneities in the time-averaged speed field [Fig. 1(a), $\mathrm{Wi} \approx 0.1$], similar to Newtonian flows [55,56]. As Wi is increased, the flow speed in fast flowing regions becomes amplified leading to "channelization" of the flow field [Fig. 1(a), $\beta = 1.0$]. In ordered geometries, the measured local temporal fluctuations [15], $\tilde{u}_{\mathrm{rms}}(\mathbf{r}) = \sqrt{\langle(\tilde{u}(\mathbf{r}, t) - \langle\tilde{u}(\mathbf{r}, t)\rangle_t)^2\rangle_t}$, of the normalized speed field, $\tilde{u}(\mathbf{r}, t) = u(\mathbf{r}, t)/U$, increase with Wi, as expected for $\mathrm{Wi} \gtrsim 1$ [Fig. 1(b), corresponding to green box in Fig. 1(a)]. In surprising contrast, the amplitude of the temporal flow speed fluctuations decreases by an order of magnitude as the disorder is increased at high Wi [Fig. 1(c), $\mathrm{Wi} \approx 4$; see also Supplemental Material, movies 1–5 [35]].

Careful inspection of the velocity field reveals that sub-pore-scale spatial fluctuations are negligible, justifying our coarse-grained, hydraulic network description of the fluctuating flow field [Figs. 2(a)–2(c)] [12]. The normalized speed fields are interpolated [Fig. 2(b)] between pillars to obtain a time dependent speed profile [Figs. 2(d) and 2(e)], $\tilde{u}(\lambda_i, t)$, where λ_i runs across throat i. Kymographs of the local throat flow speed fluctuations about the mean, $\tilde{u}' = \tilde{u}_i(t) - \langle\tilde{u}_i(t)\rangle_t$, show that their spatial extent is comparable to the pore scale [Figs. 2(d) and 2(e)]. Thus, we take the instantaneous flow speed averaged across each throat, $\tilde{u}_i(t) = \langle\tilde{u}(\lambda_i, t)\rangle_{\lambda_i}$, as our metric for speed fluctuations [Fig. 2(f)]. The normalized throat flow speed initially exhibits small fluctuations in the ordered system, which markedly grow with increasing Wi [Fig. 2(f), $\beta = 0$]. In distinct contrast, throat speeds for the disordered system remain steady for all Wi [Fig. 2(f), $\beta = 1$] with comparable fluctuations to the $\mathrm{Wi} \approx 0.1$ ordered system [Fig. 2(f), $\beta = 0$]. This pore-scale analysis captures the essential

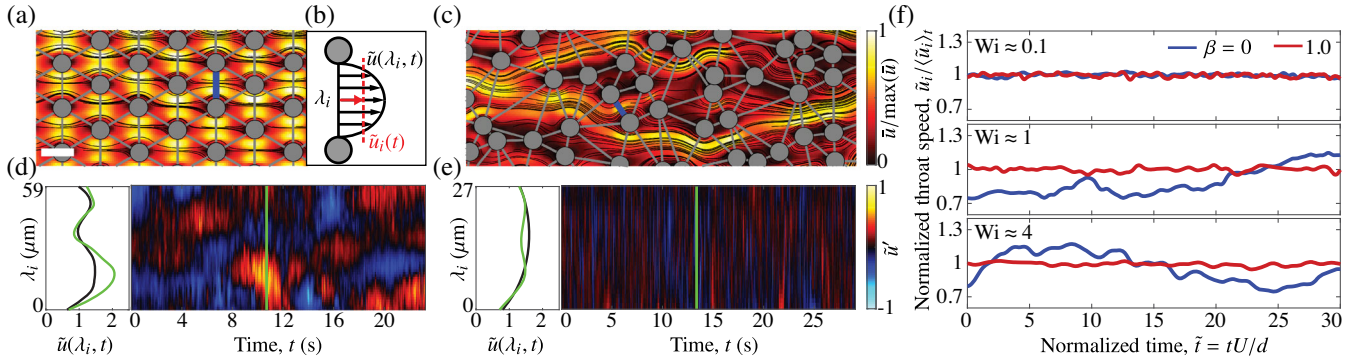

FIG. 2. Pore-scale velocity fluctuations are indicative of elastic instability. (a) Normalized, time-averaged speed field for the ordered lattice ($\beta = 0$, Wi ≈ 4). Streamlines (black) are computed from measured flow fields, and pillar locations (gray circles) are used to discretize throat cross sections (gray lines). Scale bar, 70 μm. (b) Schematic of the throat flow profile $\tilde{u}(\lambda_i, t)$ and spatially averaged speed $\tilde{u}_i(t)$ with local coordinate λ_i. (c) Normalized, time-averaged speed field for a disordered lattice ($\beta = 1$, Wi ≈ 4). (d),(e) Measured instantaneous [$\tilde{u}(\lambda_i, t)$; green] and time-averaged ($\langle\tilde{u}(\lambda_i, t)\rangle_t$; black) throat speed profiles (left) and flow speed fluctuation, $\tilde{u}_i' = \tilde{u}_i(t) - \langle\tilde{u}_i(t)\rangle_t$, kymographs (right) for individual throats from (d) ordered and (e) disordered channels [blue throats in (a) and (c), respectively; Wi ≈ 4]. Instantaneous speed profiles (left, green) correspond to indicated kymograph time (right, green). (f) Normalized, instantaneous throat flow speed for disordered ($\beta = 0$) and ordered ($\beta = 1$) throats at three different Wi values [blue throats in (a) and (c), respectively].

features of the system (Fig. 1) and provides a convenient framework to determine how disorder affects the dynamical transition to chaos.

Examination of the pore-scale flow speed fluctuations demonstrates that the onset of time dependent flow undergoes a global, forward bifurcation [12,35] in the ordered geometries but not in disordered geometries. The ensemble-averaged, temporal fluctuation of the normalized throat speeds, $\tilde{\Sigma} = \langle\sqrt{\langle(\tilde{u}_i(t) - \bar{u}_i)^2\rangle_t}\rangle_i$, is used as the order parameter, where $\bar{u}_i = \langle\tilde{u}_i(t)\rangle_t$ [Fig. 3(a)]. For the ordered lattice ($\beta = 0$) at $\mathrm{Wi}_{\mathrm{cr}} \approx 0.5$, we observe a supercritical bifurcation in the throat speed fluctuations lacking hysteresis (see Fig. S9 [35]), which is consistent with prior work in ordered arrays [12] and the predicted linear instability [9,14]. The transition is also accompanied by the onset of slow flow speed fluctuations (see Supplemental Movie 2 [35]). A minor perturbation to the ordered geometry ($\beta = 0.125$) significantly delays the transition to $\mathrm{Wi}_{\mathrm{cr}} \approx 1.2$, where time dependent flow occurs. At yet higher disorders, the transition may be delayed beyond the limits of our experiment as the flow appears stable up to Wi ≈ 5, with no discernible bifurcation for $\beta \geq 0.25$ and significantly damped speed fluctuations. For example, $\tilde{\Sigma}$ for viscoelastic flows with $\beta = 1.0$ is one order of magnitude smaller than for $\beta = 0$ and comparable to $\tilde{\Sigma}$ for both Newtonian and shear-thinning control experiments [Figs. 3(a) and 3(c); see Supplemental Material [35]]. This result represents the first observation of the stabilizing effect of disorder on viscoelastic flow. The simple scaling of $\mathrm{Wi}_{\mathrm{cr}}$ across disorders fails to predict the onset of the viscoelastic instability, indicating a deeper coupling between flow topology and polymer stretching.

As disorder suppresses the abrupt onset of temporal fluctuations, it introduces spatial heterogeneity into the flow topology [56], where viscoelasticity further enhances flow channelization (Fig. 1) [35]. The normalized, spatial throat speed fluctuations, $\tilde{\Gamma} = \sqrt{\langle(\bar{u}_i - \langle\bar{u}_i\rangle_i)^2\rangle_i}$, reveal a continuous increase with Wi from their respective, measured Newtonian values $\tilde{\Gamma}^N$ for highly disordered geometries ($\beta = [0.25, 0.5, 1.0]$) [Fig. 3(b)]. In contrast, ordered geometries ($\beta = [0, 0.125]$), where bifurcations in $\tilde{\Sigma}$ are evident, show relatively little change in $\tilde{\Gamma}$ with Wi [Fig. 3(b)]. The result is an apparent trade-off between spatial and temporal fluctuations with increasing disorder [Fig. 3(c)]. The nonlinear flow response of disordered systems to increased Wi goes beyond a simple increase in the spatial heterogeneity of flow speed, and the observed channelization [Figs. 1(a) and 2(c)] [57] alters the nature of the deformations experienced by fluid particles.

The local mode of fluid deformation, or flow type, dramatically affects the hydrodynamic response of viscoelastic fluids [58]. The flow-type parameter [59], $\Lambda = (||\mathbf{D}|| - ||\mathbf{\Omega}||)/(||\mathbf{D}|| + ||\mathbf{\Omega}||)$, quantifies the local flow kinematics ranging from pure rotation ($\Lambda = -1$) to shear ($\Lambda = 0$) to pure extension ($\Lambda = +1$), where $\mathbf{D}$ and $\mathbf{\Omega}$ are the strain rate and vorticity tensors, respectively, and $||\mathbf{D}|| = \sqrt{2\mathbf{D}:\mathbf{D}}$. At low Wi, the flow through both ordered ($\beta = 0$) and disordered ($\beta = 1$) arrays is dominated by extension [Fig. 4(a), top row]. As Wi increases, the flow type in the ordered geometry remains primarily extensional [Fig. 4(a), bottom left]. However, a clear shift toward shear-dominated flow type is evident in the disordered geometry [Fig. 4(a), bottom right], suggesting that the flow type experienced by fluid particles is integral to the stabilizing mechanism of these viscoelastic flows.

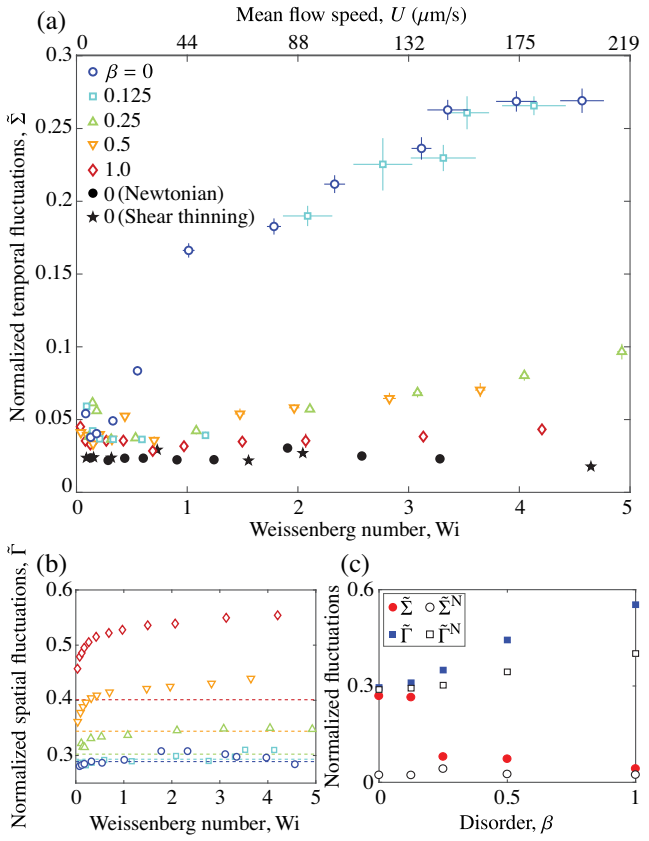

FIG. 3. Disorder delays the onset of viscoelastic instability. (a) Normalized temporal throat speed fluctuations as a function of Weissenberg number Wi for a range of geometric disorders β. Newtonian (97% glycerol; black circles) and shear-thinning (3000 ppm xanthan gum; black stars) control experiments shown for $\beta = 0$ (upper horizontal axis). (b) Normalized spatial fluctuations of time-averaged throat flow speed as a function of Wi in various disorders. Dotted lines represent measured Newtonian values. (c) Temporal and spatial fluctuations of both viscoelastic and Newtonian fluids for various β at fixed mean flow speed corresponding to Wi ≈ 4.

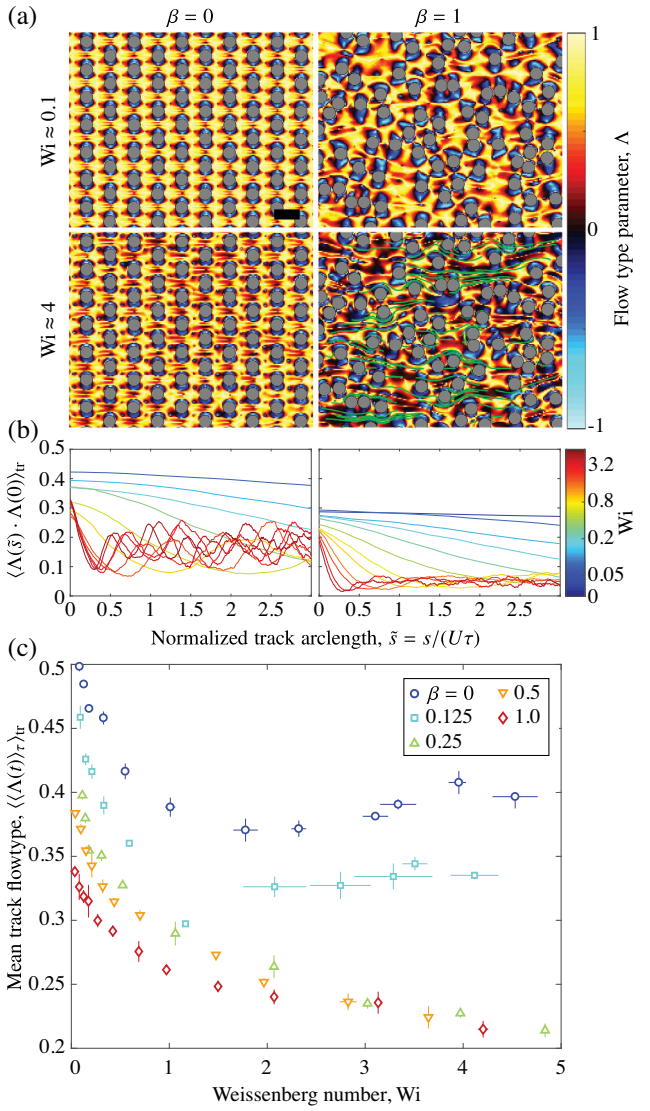

FIG. 4. Disorder regulates flow-type history and the transition to chaotic flow. (a) Flow-type parameter maps measured from time-averaged velocity fields $\bar{u}(\mathbf{r})$ for ordered and disordered channels at low and high Wi. Particle trajectories (green) shown for one relaxation time, τ (lower right). Scale bar, 100 μm. (b) Flow-type autocorrelation along tracer trajectories for $\beta = 0$ (left) and $\beta = 1$ (right). (c) Ensemble-averaged flow type along tracer trajectories over one relaxation time.

The degree of polymer stretching is dependent upon the Lagrangian flow-type history of fluid particles, which ultimately dictates the global dynamics of viscoelastic flows [60]. The autocorrelation of the flow type [Fig. 4(b)] along measured particle trajectories [Fig. 4(a), bottom right, green tracks] quantifies the constancy of fluid deformation. In ordered arrays [Fig. 4(b), left, $\beta = 0$], fluid particles are subjected to strongly extensional flow with regular frequency, whereas the weakly correlated flow type experienced in random media likely facilitates polymer relaxation [Fig. 4(b), right, $\beta = 1$] despite the spatial correlations introduced by flow channelization (Fig. 1). To compare the relative flow type experienced by fluid particles across geometries, we compute the ensemble-averaged, mean flow type (see Fig. S12 [35]) along measured particle trajectories [Fig. 4(a), bottom right] over one relaxation time τ [Fig. 4(c)]. This time-averaged flow type initially decreases with Wi for all disorders, tending toward shear. However, the most ordered geometries ($\beta = [0, 0.125]$) plateau at $\Lambda > 0.3$ for Wi $\gtrsim 1$, corresponding to the unstable regime.

Examination of the flow-type topology suggests that shear-dominated preferential paths in disordered systems globally reduce the extensional strain and the susceptibility for instability. The local flow speed negatively correlates with flow type in disordered arrays (Fig. S11 [35]): Low speed regions experience relatively strong extension, which efficiently stretches polymers and results in higher local

flow resistance [58]. Thus, as Wi increases, the system self-selects to enhance flow along low resistance preferential paths, where the locally unidirectional flows are dominated by shear that weakly stretches fluid particles. In contrast, continuity in ordered geometries frustrates the formation of preferential paths and promotes strongly curved extensional flows around pillars, which is the primary driver of viscoelastic instability [12,14]. Taken together with the Lagrangian analysis, our results show that disordered media enable viscoelastic flow to minimize extensional strain and thus stave off elastic instability, whereas ordered microstructure maintains sufficiently strong, coherent extension to trigger instability.

Lagrangian unsteady flows, having nonconstant stretch history, present theoretical challenges for understanding elastic flow instabilities [60]. The Pakdel-McKinley criterion provides some insight into the geometry-dependent conditions for elastic stability [14]:

$$\left[\frac{\tau U}{\mathcal{R}}\frac{\sigma_{11}}{\eta_0\dot{\gamma}}\right]^{1/2} \geq M_{\mathrm{cr}}, \tag{1}$$

where $\mathcal{R}$ is the radius of curvature of a streamline, σ_{11} is the streamwise tensile stress, and η_0 is the zero shear rate viscosity. The first term $\tau U/\mathcal{R}$ represents the contribution of geometry to polymer stretching through streamline curvature, but this effect has only a minor variation across disorders (see Fig. S7 in the Supplemental Material [35]). The second term in the criterion $\sigma_{11}/(\eta_0\dot{\gamma})$ is the ratio of extensional to shear stresses. While we do not have access to the local σ_{11}, the observed evolution to shear-dominated flow with increasing Wi and disorder (Fig. 4) is consistent with reducing the Pakdel-McKinley number, tending toward stable flow.

In this Letter, we demonstrate that the introduction of finite disorder into hydraulic networks suppresses the onset of chaotic velocity fluctuations associated with viscoelastic instability. The stabilizing effect of disorder is attributed to the formation of preferential flow paths, which shifts the flow-type history of fluid particles from extensional in ordered systems to shear-dominated in disordered systems. This work emphasizes the need for a Lagrangian understanding of viscoelastic flows in complex geometries beyond the Weissenberg number [14]. While the Pakdel-McKinley criterion partially accounts for flow topology, globally averaged metrics may be insufficient to predict viscoelastic stability in complex networks, underscoring the necessity for predictive theoretical tools. More broadly, coupled systems often exhibit chaotic dynamics, but few tangible examples of the counterintuitive restoration of stability by disorder have thus far been demonstrated [34]. Hence, this work provides a novel, experimental example of the suppression of chaos via disorder and adds to the growing canon of this important phenomenon.

We thank G. H. McKinley and J. Du for assistance with rheology, and P. E. Arratia, D. A. Gagnon, and A. N. Morozov for helpful discussions. This work was supported by National Science Foundation Awards No. CBET-1701392, No. CAREER-1554095, and No. CBET-1511340 (to J. S. G.).

*Corresponding author.
Jeffrey.Guasto@tufts.edu

[1] D. T. Chen, Q. Wen, P. A. Janmey, J. C. Crocker, and A. G. Yodh, Annu. Rev. Condens. Matter Phys. **1**, 301 (2010).
[2] R. G. Larson, Rheol. Acta **31**, 213 (1992).
[3] S. Gulati, D. Liepmann, and S. J. Muller, Phys. Rev. E **78**, 036314 (2008).
[4] M. Thiébaud, Z. Shen, J. Harting, and C. Misbah, Phys. Rev. Lett. **112**, 238304 (2014).
[5] M. M. Denn, AIChE J. **50**, 2335 (2004).
[6] A. Groisman and V. Steinberg, Nature (London) **410**, 905 (2001).
[7] A. Clarke, A. M. Howe, J. Mitchell, J. Staniland, L. Hawkes, and K. Leeper, Soft Matter **11**, 3536 (2015).
[8] C. Scholz, F. Wirner, J. R. Gomez-Solano, and C. Bechinger, Europhys. Lett. **107**, 54003 (2014).
[9] A. N. Morozov and W. van Saarloos, Phys. Rep. **447**, 112 (2007).
[10] T. C. Ho and M. M. Denn, J. Non-Newtonian Fluid Mech. **3**, 179 (1977).
[11] D. Bonn, F. Ingremeau, Y. Amarouchene, and H. Kellay, Phys. Rev. E **84**, 045301 (2011).
[12] L. Pan, A. Morozov, C. Wagner, and P. E. Arratia, Phys. Rev. Lett. **110**, 174502 (2013).
[13] A. Groisman and V. Steinberg, Nature (London) **405**, 53 (2000).
[14] P. Pakdel and G. H. McKinley, Phys. Rev. Lett. **77**, 2459 (1996).
[15] P. E. Arratia, C. C. Thomas, J. Diorio, and J. P. Gollub, Phys. Rev. Lett. **96**, 144502 (2006).
[16] J. Zilz, R. J. Poole, M. A. Alves, D. Bartolo, B. Levaché, and A. Lindner, J. Fluid Mech. **712**, 203 (2012).
[17] C. A. Browne, A. Shih, and S. S. Datta, Small **16**, e1903944 (2020).
[18] K. Arora, R. Sureshkumar, and B. Khomami, J. Non-Newtonian Fluid Mech. **108**, 209 (2002).
[19] A. Varshney and V. Steinberg, Phys. Rev. Fluids **2**, 051301 (2017).
[20] S. J. Muller, R. G. Larson, and E. S. G. Shaqfeh, Rheol. Acta **28**, 499 (1989).
[21] G. H. McKinley, R. C. Armstrong, and R. A. Brown, Phil. Trans. R. Soc. A **344**, 265 (1993).
[22] P. C. Sousa, F. T. Pinho, M. S. N. Oliveira, and M. A. Alves, Soft Matter **11**, 8856 (2015).
[23] B. Qin and P. E. Arratia, Phys. Rev. Fluids **2**, 083302 (2017).
[24] J. A. Deiber and W. R. Schowalter, AIChE J. **27**, 912 (1981).
[25] R. J. Poole, M. A. Alves, and P. J. Oliveira, Phys. Rev. Lett. **99**, 164503 (2007).
[26] M. Grilli, A. Vázquez-Quesada, and M. Ellero, Phys. Rev. Lett. **110**, 174501 (2013).

[27] P. W. Anderson, Phys. Rev. **109**, 1492 (1958).
[28] E. R. Weeks and D. A. Weitz, Phys. Rev. Lett. **89**, 095704 (2002).
[29] D. J. Watts and S. H. Strogatz, Nature (London) **393**, 440 (1998).
[30] Y. Braiman, J. F. Lindner, and W. L. Ditto, Nature (London) **378**, 465 (1995).
[31] W. L. Shew, H. A. Coy, and J. F. Lindner, Am. J. Phys. **67**, 703 (1999).
[32] N. Mousseau, Phys. Rev. Lett. **77**, 968 (1996).
[33] A. J. Fontenele, N. A. P. de Vasconcelos, T. Feliciano, L. A. A. Aguiar, C. Soares-Cunha, B. Coimbra, L. Dalla Porta, S. Ribeiro, A. J. Rodrigues, N. Sousa, P. V. Carelli, and M. Copelli, Phys. Rev. Lett. **122**, 208101 (2019).
[34] F. Sagués, J. M. Sancho, and J. García-Ojalvo, Rev. Mod. Phys. **79**, 829 (2007).
[35] See Supplemental Material at http://link.aps.org/supplemental/10.1103/PhysRevLett.124.164501, which includes Refs. [36–53], for details about experimental methods, and supplemental figures and movies.
[36] N. T. Ouellette, P. J. J. O'Malley, and J. P. Gollub, Phys. Rev. Lett. **101**, 174504 (2008).
[37] C. Faustino, A. F. Bettencourt, A. Alfaia, and L. Pinheiro, J. Chem. Educ. **92**, 936 (2015).
[38] R. Christensen, *Theory of Viscoelasticity: An Introduction* (Academic Press, New York, 1971).
[39] R. Bird, R. Armstrong, and O. Hassager, *Dynamics of Polymeric Liquids, Volume 1: Fluid Mechanics* (Wiley, New York, 1987).
[40] S. L. Anna and G. H. McKinley, J. Rheol. **45**, 115 (2001).
[41] J. P. Rothstein and G. H. McKinley, J. Non-Newtonian Fluid Mech. **86**, 61 (1999).
[42] J. P. Rothstein and G. H. McKinley, J. Non-Newtonian Fluid Mech. **98**, 33 (2001).
[43] V. Entov and E. Hinch, J. Non-Newtonian Fluid Mech. **72**, 31 (1997).
[44] A. E. Koser, L. Pan, N. C. Keim, and P. E. Arratia, Lab Chip **13**, 1850 (2013).
[45] J. L. Amundarain, L. J. Castro, M. R. Rojas, S. Siquier, N. Ramírez, A. J. Müller, and A. E. Sáez, Rheol. Acta **48**, 491 (2009).
[46] L. Casanellas, M. A. Alves, R. J. Poole, S. Lerouge, and A. Lindner, Soft Matter **12**, 6167 (2016).
[47] F. Zami-Pierre, R. de Loubens, M. Quintard, and Y. Davit, J. Non-Newtonian Fluid Mech. **261**, 99 (2018).
[48] S. Whitaker, Transp. Porous Media **1**, 3 (1986).
[49] D. Kawale, G. Bouwman, S. Sachdev, P. L. J. Zitha, M. T. Kreutzer, W. R. Rossen, and P. E. Boukany, Soft Matter **13**, 8745 (2017).
[50] D. Kawale, E. Marques, P. L. J. Zitha, M. T. Kreutzer, W. R. Rossen, and P. E. Boukany, Soft Matter **13**, 765 (2017).
[51] A. Groisman and V. Steinberg, New J. Phys. **6**, 29 (2004).
[52] A. Fouxon and V. Lebedev, Phys. Fluids **15**, 2060 (2003).
[53] P. G. De Gennes, J. Chem. Phys. **60**, 5030 (1974).
[54] W. Thielicke and E. J. Stamhuis, J. Open Res. Software **2**, e30 (2014).
[55] K. Alim, S. Parsa, D. A. Weitz, and M. P. Brenner, Phys. Rev. Lett. **119**, 144501 (2017).
[56] N. Stoop, N. Waisbord, V. Kantsler, V. Heinonen, J. S. Guasto, and J. Dunkel, J. Non-Newtonian Fluid Mech. **268**, 66 (2019).
[57] S. S. Datta, H. Chiang, T. S. Ramakrishnan, and D. A. Weitz, Phys. Rev. Lett. **111**, 064501 (2013).
[58] D. E. Smith, H. P. Babcock, and S. Chu, Science **283**, 1724 (1999).
[59] G. Astarita, J. Non-Newtonian Fluid Mech. **6**, 69 (1979).
[60] C. E. Wagner and G. H. McKinley, J. Non-Newtonian Fluid Mech. **233**, 133 (2016).